ACS APPLIED MATERIALS & INTERFACES

Research Article

www.acsami.org

Large-Scale Roll-to-Roll Fabrication of Ordered Mesoporous Materials using Resol-Assisted Cooperative Assembly

Zhe Qiang,[†] Yuanhao Guo,[†] Hao Liu,[‡] Stephen Z.D. Cheng,[‡] Miko Cakmak,[†] Kevin A. Cavicchi,[†] and Bryan D. Vogt*,[†]

[†]Department of Polymer Engineering, The University of Akron, 250 South Forge Street, Akron, Ohio 44325, United States

[‡]Department of Polymer Science, Goodyear Polymer Center, The University of Akron, 170 University Circle, Akron, Ohio 44325, United States

Supporting Information

ABSTRACT: Roll-to-roll (R2R) processing enables the rapid fabrication of large-area sheets of cooperatively assembled materials for production of mesoporous materials. Evaporation induced self-assembly of a nonionic surfactant (Pluronic F127) with sol−gel precursors and phenolic resin oligomers (resol) produce highly ordered mesostructures for a variety of chemistries including silica, titania, and tin oxide. The cast thick (>200 μm) film can be easily delaminated from the carrier substrate (polyethylene terephthalate, PET) after cross-linking the resol to produce meter-long self-assembled sheets. The surface areas of these mesoporous materials range from 240 m^2/g to >1650 m^2/g with these areas for each material comparing favorably with prior reports in the literature. These R2R methods provide a facile route to the scalable production of kilograms of a wide variety of ordered mesoporous materials that have shown potential for a wide variety of applications with small-batch syntheses.

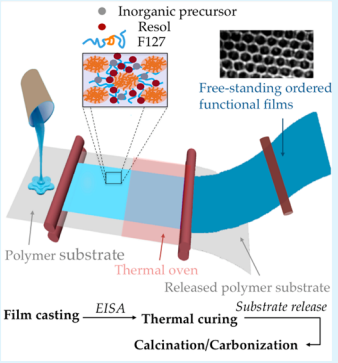

KEYWORDS: *SBA-15, FDU-15, titania, tin oxide, nanocomposite, continuous production*

INTRODUCTION

Ordered mesoporous materials, fabricated by soft-templating with an amphiphile, hold significant potential for a broad range of applications, including supercapacitors,[1] drug delivery,[2] biosensing,[3] and energy storage.[4,5] In particular, a wealth of possible materials are available from the facile templating of nonionic block copolymers by sol−gel: metal oxides[6] and metals,[7] nanoparticles,[8] or even composites.[9] However, the fabrication of these mesoporous materials is generally by batch processes and scale-up requires larger vessels, but the container size can impact the mesostructure that develops.[10] For the synthesis of mesoporous carbon on the kilogram scale, polyurethane (PU) foam was used as a 3D scaffold,[11] but this method has not been extended to other mesoporous materials. Moreover, the synthesis is limited by the drying of the templating solution in the PU pores. Thus, development of a more scalable and generalized approach for the continuous production of various mesoporous materials could be enabling for commercial production.

There is significant economic incentive to transfer production from batch to continuous processes because of improved efficiencies. For production of chemicals, this is commonly accomplished through flow reactors,[12] but this geometry is commonly not suitable for the fabrication of new materials. However, for functional materials, roll-to-roll (R2R) processing is one promising technique for their continuous fabrication including examples for food packaging,[13] semiconductors,[14] organic photovoltaics,[15] and nanostructured features via nanoimprint lithography.[16,17] R2R enables low cost production and is highly scalable. Recently, the R2R technique has been extended to the synthesis of flexible carbon transparent electrodes[18] and highly ionic conductive membranes.[19] However, one limitation of R2R is the challenge associated with scale up from lab-scale processing to the large-scale production.[20]

Herein, we report the continuous fabrication of a wide variety of mesoporous materials via R2R processing using a 21 m long R2R machine that enables casting and curing of the film. We apply a resol (phenolic resin)-assisted assembly method to limit the sensitivity to the ambient humidity. Moreover, the thermal cross-linking of the resol delaminates the cooperatively assembled film from the thermally stabilized polyethylene terephthalate (PET) substrate, which enables the fabrication of freestanding thick (~200 μm) films that are meters long. Calcination/carbonization of these films produce large quantities of mesoporous materials with similar or improved material properties (surface area, pore size, degree of order) compared to analogous materials from small batch syntheses.

Received: December 11, 2014
Accepted: January 30, 2015
Published: January 30, 2015

DOI: 10.1021/am5086275
ACS Appl. Mater. Interfaces 2015, 7, 4306−4310

EXPERIMENTAL SECTION

Materials. Phenol (>99%), formaldehyde (ACS reagent, 37 wt % in H_2O, contains 10−15% methanol as stabilizer), titanium(IV) chloride (>99%), tin(IV) chloride (>99%), ethanol (>99%), Pluronic F127, tetraethyl orthosilicate (>98%), and potassium hydroxide (>85%) were purchased from Sigma-Aldrich. Polyethylene terephthalate (PET) sheet was purchased from Terphane Inc. A low-molecular-weight phenolic resin (resol) was synthesized by NaOH-catalyzed condensation as previously reported.[21]

Synthesis of Mesoporous Carbon-Silica/Mesoporous Carbon/Mesoporous Silica. The mesoporous carbon-silica nanocomposite was synthesized to match previously reported MP-CS-46.[22] Briefly, 160 g of the Pluronic F127 was initially dissolved in 50 g of 0.2 M HCl and 400 g of ethanol. After stirring for 2 h, 100 g of tetraethyl orthosilicate (TEOS) and 100 g of resol-ethanol solution (50 wt % in ethanol) were added into this solution and stirred for another 2 h at 40 °C. Doctor blade solution casting was utilized to fabricate a 400 μm thick triconstituent solution film on a thermally stabilized PET substrate moving at 50 cm/min using a custom R2R machine (see Figure S1 in the Supporting Information for images of the coating instrument). The residual ethanol was removed at 50 °C for 1 h, and subsequently the resol was cross-linked at 120 °C for 2 h. The thermopolymerized film was peeled from the PET substrate. To fit the material in the tube furnace (SentroTech Corp.), the thick film was broke into pieces and placed in a large alumina boat (Anderman Ceramics, Inc.) before being carbonized at 800 °C for 3 h in N_2. The heat schedule for carbonization was 1 °C/min to 600 and 5 °C/min to 800 °C. For the mesoporous carbon, the carbonized materials were etched with 3 mol/L KOH ethanoic solution. For mesoporous silica, the carbonized films were calcinated at 500 °C in air for 3 h.

Synthesis of Mesoporous Metal Oxides. A stock $TiCl_4$ or $SnCl_4$ solution was prepared by mixing the metal chloride (20 wt %) with ethanol and deionized water (70:30 w/w) under vigorous stirring for 30 min. For a typical synthesis, 30 g of F127 was dissolved in 100 g of anhydrous-ethanol. Twenty-five grams of the 20 wt % resol-ethanol solution and 15 g of the 20 wt % metal chloride solution were mixed and stirred for 1 h. The solution was then doctor blade coated onto the PET substrate at 50 cm/min. The films were heated at 60 °C for 1 h and subsequently at 120 °C for 2 h prior to calcination at 500 °C for 3 h. For calcination, the temperature was increased and decreased at 1 °C/min from ambient temperature to 500 °C.

Characterization. Fourier transform infrared spectroscopy (Thermo Scientific iS50 FT-IR) was performed to determine the composition of the films. Transmission small-angle X-ray scattering (SAXS) was performed on a Rigaku MicroMax 002+ instrument with a 2D multiwire area detector and a sealed copper tube operating at 45 kV to produce 0.154 nm X-rays. The scattering vector (q) was calibrated using silver behenate with the primary reflection peak at q = 1.067 nm^{-1}. Two-dimensional SAXS patterns were collected over 0.12 < q < 2 nm^{-1}. A JEOL-1230 transmission electron microscope (TEM) with an accelerating voltage of 120 kV was utilized to record the bright field images using a digital CCD camera. In order to determine the textural properties, N_2 adsoprtion and desorption isotherms were measured using a Micromeritics Tristar. The pore size distributions were calculated from the adsorption isotherms using the Barrett, Joyner and Halenda (BJH) model, whereas the surface area was determined from the typical Brunauer Emmett and Teller (BET) analysis. The framework density was measured by using helium pycnometer (Micomeritics AccuPyc II 1340). Powder X-ray diffraction (XRD) (Bruker AXS D8 discover system) was used to to examine the crystalline phase of mesoporous metal oxides. Optical images were taken using a Canon 5D Mark II camera with a 200 mm lens.

RESULTS AND DISCUSSION

Figure 1A shows a schematic of the roll-to-roll processing machine, which is used to produce 15 cm wide functional films. This processing line consists of doctor blade coating of the functional solution and two different oven zones for solvent evaporation and thermal annealing to cross-link the resol,

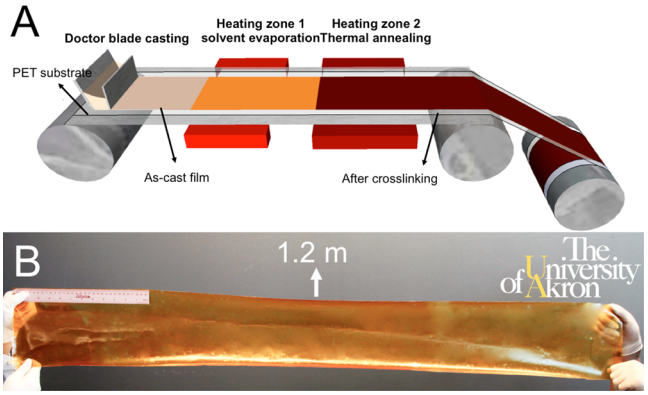

Figure 1. (A) Schematic illustrator of roll-to-roll machine combining a doctor blade for thin film coating and two ovens for solvent evaporation and thermal annealing respectively; (B) real photo of 1.2 m long, 200 μm free-standing F127:TEOS:resol film after thermal cross-linking.

respectively. Herein, we demonstrate this approach for the fabrication of mesoporous carbon, silica, titania, and tin oxide. A triconstituent coassembly approach based on the evaporation-induced assembly of a polymeric solution (resol, sol gel precursor, and Pluronic F127) is used for the fabrication. The precursor solution is cast by doctor blade onto the moving polyethylene terephthalate (PET) substrate at 50 cm/min to generate an initial wet film thickness of around 400 μm. One key consideration is the thickness of the cast film: the material yield per area increases with increasing coating thickness, but we have found that ordering of the material is significantly compromised for wet thicknesses significantly exceeding 500 μm (see Figure S2 in the Supporting Information). Therefore, an initial wet film thickness of approximately 400 μm was used in all cases presented here. Unlike dip coating,[23] the speed of the film casting does not significantly impact the ordered structure as long as the residence times for drying and cross-linking of the resol remains constant. The cast film is carried by the PET substrate to an 50 °C oven zone (zone #1 in Figure 1A) in order to evaporate the residual solvent for 1 h. Subsequently, the resol in the film is cross-linked at 120 °C by translation through zone #2 for 2 h. This temperature is selected to enable near complete resol cross-linking within 2 h.[24] Prior work has demonstrated that the ordered structure is generated on evaporation for TEOS-resol mixtures,[25,26] so the properties of the mesoporous materials are not strongly dependent on the cross-linking temperature. After the resol is cross-linked, the polymeric film can be simply peeled off from the PET substrate. We hypothesize that the contraction of the resol during cross-linking leads to internal stresses that weaken the adhesion between the cast film and the PET substrate. Simply bending the laminated film near an edge leads to delamination; peeling this loose edge from the PET leads to a free-standing film. Figure 1B shows a free-standing, cross-linked, cooperatively assembled film approximately 200 μm thick × 1.2 m long × 0.15 m wide.

Carbonization of these materials at 800 °C removes the block copolymer template (Pluronic F127) to produce an ordered mesoporous carbon-silica (OMCS) nanocomposite. The carbonization is confirmed by the FTIR (Figure S3 in the Supporting Information). The powder yield for the OMCS is approximately 20−30 g/m^2. Simply varying the length of the film cast can control the total amount of material produced

DOI: 10.1021/am5086275
ACS Appl. Mater. Interfaces 2015, 7, 4306−4310

during the R2R processing. We have produced more than 100 g and as little as 1 g with this R2R process without significant variance in the pore properties of the mesoporous material. Figure 2A shows the large domains of highly ordered cylindrical

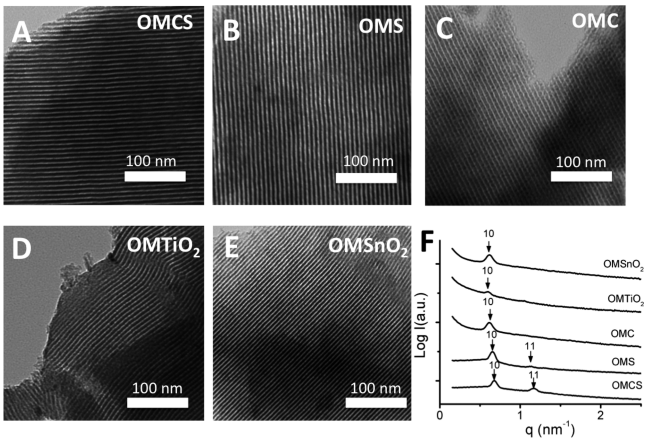

Figure 2. TEM images of ordered mesoporous (A) carbon–silica, (B) silica, (C) carbon, (D) titanium dioxide, and (E) tin oxide. (F) SAXS profiles of corresponding materials further demonstrate their ordered nature. These materials are powders obtained from the large cooperatively assembled sheets.

mesopores of the OMCS. Small-angle X-ray scattering (SAXS) confirms this morphology from the two well-resolved diffraction peaks indexed to 10 and 11 reflections associated with two-dimensional hexagonal packing (Figure 2F). The lattice parameter determined from the primary peak of SAXS is approximately 10.2 nm, which is consistent with small batch synthesis.[22] Calcination of the OMCS nanocomposite at 500 °C in air, removes the carbon to generate an ordered mesoporous silica (OMS). As shown by TEM (Figure 2B), the ordered mesostructure is preserved through calcination process. From SAXS (Figure 2F), the lattice parameter decreases to 9.7 nm because of framework shrinkage during calcination. Alternatively, the OMCS can be converted to ordered mesoporous carbon (OMC) by etching the silica framework in ethanoic KOH without loss of the mesostructure as confirmed by TEM (Figure 2C) and SAXS (Figure 2F).

This R2R processing can be applied to the general fabrication of ordered mesoporous metal oxides (OMM) using the sol–gel method. Addition of resol in the precursor can reduce the aging time[27] of the sol–gel precursor from 1–7 days[28] to 1 h for these studies. Following a similar protocol to fabrication of the silica, but using titanium chloride as precursor, produces mesoporous TiO_2 after cross-linking the resol at 120 °C and subsequent calcination at 500 °C. In this case, approximately 20 g/m^2 of mesoporous TiO_2 is obtained from the cross-linked sheet produced by R2R. This productivity for material fabrication should scale with the density of the framework, but the resol is fully removed in this case, which decreases the amount of mesoporous material obtained from the cross-linked sheet. Figure 2D illustrates the highly ordered cylindrical mesostructure of mesoporous TiO_2, with a lattice parameter of 11.2 nm from SAXS (Figure 2F). Additionally, this resol-assisted assembly can be applied to materials that are difficult to fabricate such as ordered mesoporous tin oxide ($OMSnO_2$). The competition between kinetics of reorganization and hydrolysis requires delayed humidity treatments to control the formation of the SnO_2 mesotructures.[29] We can avoid this complication by incorporation of resol to generate highly ordered nanostructures in $OMSnO_2$ as determined by TEM (Figure 2E) and SAXS (Figure 2F).

Figure 3A shows the N_2 sorption isotherms for the ordered mesoporous materials. All these materials exhibit type-IV

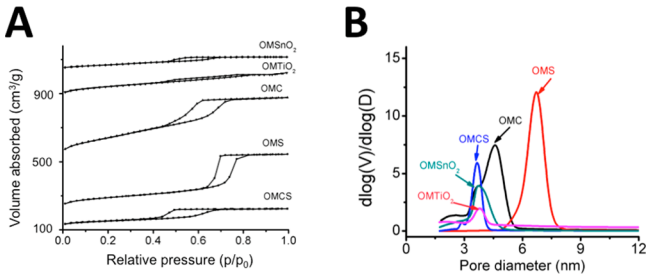

Figure 3. (A) Nitrogen adsorption–desorption isotherms for OMCS, OMC, OMS, $OMTiO_2$, and $OMSnO_2$ and (B) its corresponding pore size distribution. The isotherms are vertically offset by 150, 250, 750, and 1000 cm^3/g for OMS, OMS, $OMTiO_2$, and $OMSnO_2$, respectively.

isotherms with a hysteresis loop as expected for an ordered mesoporous materials with cylindrical (*p6mm*) pores.[30] However, despite the same block copolymer template used in each case, there are significant differences in the isotherms. First, the OMC and OMS are daughters of the OMCS from the selective removal of the silica and carbon, respectively. The pore size calculated using the Barrett–Joyner–Halenda (BJH) model increases from approximately 4.3 nm for OMCS to 4.8 nm (OMC) and 6.9 nm (OMS) with this selective removal (Figure 3B). The increase in the pore size is similar to the prior report for analogous materials processed in batch.[22] Similarly, the surface area determined by Brunauer–Emmett–Teller (BET)[31] methodology increases significantly from 445 m^2/g (OMCS) to 1658 m^2/g (OMC) because of the introduction of micropores by removal of the silica from the carbon-silica framework of the OMCS. Table 1 summarizes the pore characteristics of these materials.

Table 1. Material Properties of the Mesoporous Materials Prepared by Roll-to-Roll Processing Methods

materials	lattice parameter (nm)	pore size (nm)	BET surface area (m^2/g)	framework density (g/cm^3)
OMCS	9.2	4.3	445	2.15
OMS	9.7	6.9	657	2.16
OMC	10.1	6.0	1658	2.14
$OMTiO_2$	11.2	4.6	360	3.79
$OMSnO_2$	10.6	4.4	244	6.71

The hysteresis loops in the isotherms for the $OMTiO_2$ and $OMSnO_2$ are similar to each other (Figure 3A), but appears to not be as well-defined as the other materials. This difference in the hysteresis loops is partially due to the decreased sorption capacity of these metal oxides (specific volume adsorbed) and the associated much larger framework density for $OMTiO_2$ and $OMSnO_2$, which will increase the mass for a given volume to decrease the specific volume. Nonetheless, the pore size distribution is narrow and well-defined (Figure 3B). The average pore size is similar for these two metal oxides and the OMCS as expected for the same template. In addition to decreasing the sensitivity to ambient humidity,[27] the incorpo-

DOI: 10.1021/am5086275
ACS Appl. Mater. Interfaces 2015, 7, 4306–4310

ration of resol acts to increase the surface area by introduction of micropores in the framework during calcination. The surface area of the $OMTiO_2$ (~360 m^2/g) is much greater than typically reported,[32] especially for calcination at high temperatures where this resol-assisted method nearly doubles the surface area.[32] For applications such as dye-sensitized solar cells (DSSC), this improvement in the surface area of $OMTiO_2$ should be highly beneficial for high efficiencies. Similarly, the surface area of $OMSnO_2$ is significantly higher than previous reports using only sol gel processing.[28] The length of the thick film produced controls the quantity of material produced without changing any other processing conditions or adversely impacting material properties, unlike the decrease in surface area obtained for the kilogram scale synthesis of mesoporous carbons using PU foams.[11] Moreover, the framework density of $OMTiO_2$ is consistent with high crystallinity (bulk anatase = 3.79 g/cm^3). Figure 4 illustrates the XRD profiles for the

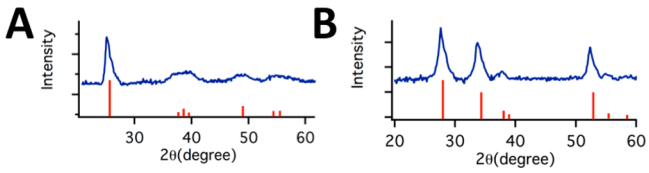

Figure 4. XRD profiles for (A) $OMTiO_2$ and (B) $OMSnO_2$. The diffraction peaks are consistent with anatase for TiO_2 and cassiterite for SnO_2 as shown by the red lines.

$OMTiO_2$ and $OMSnO_2$. This result confirms highly crystalline anatase phase of the TiO_2 and cassiterite phase for SnO_2, which is consistent with previous reports.[33,34]

CONCLUSIONS

The general applicability of roll-to-roll processing methodology based on the resol-assisted assembly has been demonstrated for the potential continuous fabrication of a wide variety of mesoporous materials. This processing should be capable of meeting commercial requirements for low cost fabrication with flexibility to generate materials on demand in quantities from the gram scale to many kilograms. Additionally, inclusion of resol in the precursor solution appears to improve the properties of the porous materials (pore size uniformity and surface area) and decreases the environmental sensitivity during fabrication. This on-demand fabrication of tunable quantities could prove powerful for the screening of different mesoporous materials in a variety of applications.

ASSOCIATED CONTENT

Supporting Information

Pictures of the roll-to-roll machine for casting, annealing, and controlled take-up of the web; FTIR of mesoporous carbon-silica film; diffraction data from SAXS for each of the individual materials. This material is available free of charge via the Internet at http://pubs.acs.org

AUTHOR INFORMATION

Corresponding Author

*E-mail: vogt@uakron.edu.

Author Contributions

The manuscript was written through contributions of all authors. All authors have given approval to the final version of the manuscript.

Notes

The authors declare no competing financial interest.

ACKNOWLEDGMENTS

This work was supported by the National Science Foundation under Grant 1159295. The authors thank Dr. Sadhan Jana and Senlong Gu for use of the helium pycnometer. The authors acknowledge Jeongwoo Lee for the helpful discussion.

REFERENCES

(1) Zhai, Y. P.; Dou, Y. Q.; Zhao, D. Y.; Fulvio, P. F.; Mayes, R. T.; Dai, S. Carbon Materials for Chemical Capacitive Energy Storage. *Adv. Mater.* **2011**, *23*, 4828−4850.

(2) Zhu, J.; Liao, L.; Bian, X.; Kong, J.; Yang, P.; Liu, B. pH-Controlled Delivery of Doxorubicin to Cancer Cells, Based on Small Mesoporous Carbon Nanospheres. *Small* **2012**, *8*, 2715−2720.

(3) Slowing, I. I.; Trewyn, B. G.; Giri, S.; Lin, V. S. Y. Mesoporous Silica Nanoparticles for Drug Delivery and Biosensing Applications. *Adv. Funct. Mater.* **2007**, *17*, 1225−1236.

(4) Li, Y.; Tan, B.; Wu, Y. Mesoporous Co_3O_4 Nanowire Arrays for Lithium Ion Batteries with High Capacity and Rate Capability. *Nano Lett.* **2008**, *8*, 265−270.

(5) Fan, J.; Wang, T.; Yu, C. Z.; Tu, B.; Jiang, Z. Y.; Zhao, D. Y. Ordered, Nanostructured Tin-based Oxides/Carbon Composite as the Negative-Electrode Material for Lithium-Ion Batteries. *Adv. Mater.* **2004**, *16*, 1432−1436.

(6) Yang, P. D.; Zhao, D. Y.; Margolese, D. I.; Chmelka, B. F.; Stucky, G. D. Generalized Syntheses of Large-Pore Mesoporous Metal Oxides with Semicrystalline Frameworks. *Nature* **1998**, *396*, 152−155.

(7) Warren, S. C.; Perkins, M. R.; Adams, A. M.; Kamperman, M.; Burns, A. A.; Arora, H.; Herz, E.; Suteewong, T.; Sai, H.; Li, Z.; Werner, J.; Song, J.; Werner-Zwanziger, U.; Zwanziger, J. W.; Graetzel, M.; DiSalvo, F. J.; Wiesner, U. A Silica Sol-Gel Design Strategy for Nanostructured Metallic Materials. *Nat. Mater.* **2012**, *11*, 460−467.

(8) Zhang, Q.; Wang, X.; Li, P.-Z.; Kim Truc, N.; Wang, X.-J.; Luo, Z.; Zhang, H.; Tan, N. S.; Zhao, Y. Biocompatible, Uniform, and Redispersible Mesoporous Silica Nanoparticles for Cancer- Targeted Drug Delivery In Vivo. *Adv. Funct. Mater.* **2014**, *24*, 2450−2461.

(9) Fang, Y.; Zheng, G.; Yang, J.; Tang, H.; Zhang, Y.; Kong, B.; Lv, Y.; Xu, C.; Asiri, A. M.; Zi, J.; Zhang, F.; Zhao, D. Dual-Pore Mesoporous Carbon@ Silica Composite Core- Shell Nanospheres for Multidrug Delivery. *Angew. Chem., Int. Ed.* **2014**, *53*, 5366−5370.

(10) Sun, X.; Shi, Y.; Zhang, P.; Zheng, C.; Zheng, X.; Zhang, F.; Zhang, Y.; Guan, N.; Zhao, D.; Stucky, G. D. Container Effect in Nanocasting Synthesis of Mesoporous Metal Oxides. *J. Am. Chem. Soc.* **2011**, *133*, 14542−14545.

(11) Wang, J.; Xue, C.; Lv, Y.; Zhang, F.; Tu, B.; Zhao, D. Kilogram-Scale Synthesis of Ordered Mesoporous Carbons and Their Electrochemical Performance. *Carbon* **2011**, *49*, 4580−4588.

(12) Mason, B. P.; Price, K. E.; Steinbacher, J. L.; Bogdan, A. R.; McQuade, D. T. Greener Approaches to Organic Synthesis using Microreactor Technology. *Chem. Rev.* **2007**, *107*, 2300−2318.

(13) Kang, H.; Park, H.; Park, Y.; Jung, M.; Kim, B. C.; Wallace, G.; Cho, G. Fully Roll-to-Roll Gravure Printable Wireless (13.56 MHz) Sensor-Signage Tags for Smart Packaging. *Sci. Rep.* **2014**, *4*, 5387.

(14) Diao, Y.; Tee, B. C. K.; Giri, G.; Xu, J.; Kim, D. H.; Becerril, H. A.; Stoltenberg, R. M.; Lee, T. H.; Xue, G.; Mannsfeld, S. C. B.; Bao, Z. Solution Coating of Large-Area Organic Semiconductor Thin Films with Aligned Single-Crystalline Domains. *Nat. Mater.* **2013**, *12*, 665−671.

(15) Sondergaard, R.; Manceau, M.; Jorgensen, M.; Krebs, F. C. New Low-Bandgap Materials with Good Stabilities and Efficiencies Comparable to P3HT in R2R-Coated Solar Cells. *Adv. Energy Mater.* **2012**, *2*, 415−418.

(16) Ahn, S. H.; Guo, L. J. High-Speed Roll-to-Roll Nanoimprint Lithography on Flexible Plastic Substrates. *Adv. Mater.* **2008**, *20*, 2044−2049.

DOI: 10.1021/am5086275
ACS Appl. Mater. Interfaces 2015, 7, 4306−4310

(17) Ahn, S. H.; Guo, L. J. Large-Area Roll-to-Roll and Roll-to-Plate Nanoimprint Lithography: A Step toward High-Throughput Application of Continuous Nanoimprinting. *ACS Nano* **2009**, *3*, 2304−2310.
(18) Hu, X.; Chen, L.; Zhang, Y.; Hu, Q.; Yang, J.; Chen, Y. Large-Scale Flexible and Highly Conductive Carbon Transparent Electrodes via Roll-to-Roll Process and Its High Performance Lab-Scale Indium Tin Oxide-Free Polymer Solar Cells. *Chem. Mater.* **2014**, *26*, 6293−6302.
(19) Batra, S.; Unsal, E.; Cakmak, M. Directed Electric Field Z-Alignment Kinetics of Anisotropic Nanoparticles for Enhanced Ionic Conductivity. *Adv. Funct. Mater.* **2014**, *24*, 7698−7708.
(20) Søndergaard, R. R.; Hösel, M.; Krebs, F. C. Roll-to-Roll Fabrication of Large Area Functional Organic Materials. *J. Polym. Sci., Part B: Polym. Phys.* **2013**, *51*, 16−34.
(21) Meng, Y.; Gu, D.; Zhang, F. Q.; Shi, Y. F.; Yang, H. F.; Li, Z.; Yu, C. Z.; Tu, B.; Zhao, D. Y. Ordered Mesoporous Polymers and Homologous Carbon Frameworks: Amphiphilic Surfactant Templating and Direct Transformation. *Angew. Chem., Int. Ed.* **2005**, *44*, 7053−7059.
(22) Liu, R. L.; Shi, Y. F.; Wan, Y.; Meng, Y.; Zhang, F. Q.; Gu, D.; Chen, Z. X.; Tu, B.; Zhao, D. Y. Triconstituent Co-Assembly to Ordered Mesostructured Polymer-Silica and Carbon-Silica Nanocomposites and Large-Pore Mesoporous Carbons with High Surface Areas. *J. Am. Chem. Soc.* **2006**, *128*, 11652−11662.
(23) Sanchez, C.; Boissiere, C.; Grosso, D.; Laberty, C.; Nicole, L. Design, Synthesis, and Properties of Inorganic and Hybrid Thin Films Having Periodically Organized Nanoporosity. *Chem. Mater.* **2008**, *20*, 682−737.
(24) Zhang, Y. Z.; Qiang, Z.; Vogt, B. D. Relationship between Crosslinking and Ordering Kinetics for the Fabrication of Soft Templated (FDU-16) Mesoporous Carbon Thin Films. *RSC Adv.* **2014**, *4*, 44858−44867.
(25) Song, L.; Feng, D.; Campbell, C. G.; Gu, D.; Forster, A. M.; Yager, K. G.; Fredin, N.; Lee, H.-J.; Jones, R. L.; Zhao, D.; Vogt, B. D. Robust Conductive Mesoporous Carbon-Silica Composite Films with Highly Ordered and Oriented Orthorhombic Structures from Triblock-Copolymer Template Co-Assembly. *J. Mater. Chem.* **2010**, *20*, 1691−1701.
(26) Song, L. Y.; Feng, D.; Lee, H. J.; Wang, C. Q.; Wu, Q. Y.; Zhao, D. Y.; Vogt, B. D. Stabilizing Surfactant Templated Cylindrical Mesopores in Polymer and Carbon Films through Composite Formation with Silica Reinforcement. *J. Phys. Chem. C* **2010**, *114*, 9618−9626.
(27) Luo, W.; Li, Y.; Dong, J.; Wei, J.; Xu, J.; Deng, Y.; Zhao, D. A Resol-Assisted Co-Assembly Approach to Crystalline Mesoporous Niobia Spheres for Electrochemical Biosensing. *Angew. Chem., Int. Ed.* **2013**, *52*, 10505−10510.
(28) Yang, P. D.; Zhao, D. Y.; Margolese, D. I.; Chmelka, B. F.; Stucky, G. D. Block Copolymer Templating Syntheses of Mesoporous Metal Oxides with Large Ordering Lengths and Semicrystalline Framework. *Chem. Mater.* **1999**, *11*, 2813−2826.
(29) Urade, V. N.; Hillhouse, H. W. Synthesis of Thermally Stable Highly Ordered Nanoporous Tin Oxide Thin Films with a 3D Face-Centered Orthorhombic Nanostructure. *J. Phys. Chem. B* **2005**, *109*, 10538−10541.
(30) Sakamoto, Y.; Kim, T. W.; Ryoo, R.; Terasaki, O. Three-Dimensional Structure of Large-Pore Mesoporous Cubic Ia(3)Over-Bard Silica with Complementary Pores and its Carbon Replica by Electron Crystallography. *Angew. Chem., Int. Ed.* **2004**, *43*, 5231−5234.
(31) Brunauer, S.; Emmett, P. H.; Teller, E. Adsorption of Gases in Multimolecular Layers. *J. Am. Chem. Soc.* **1938**, *60*, 309−318.
(32) Choi, S. Y.; Mamak, M.; Coombs, N.; Chopra, N.; Ozin, G. A. Thermally Stable Two-Dimensional Hexagonal Mesoporous Nanocrystalline Anatase, Meso-Nc-Tio_2: Bulk and Crack-Free Thin Film Morphologies. *Adv. Funct. Mater.* **2004**, *14*, 335−344.
(33) Bai, H.; Li, X.; Hu, C.; Zhang, X.; Li, J.; Yan, Y.; Xi, G. Large-Scale, Three-Dimensional. Free-Standing, and Mesoporous Metal Oxide Networks for High-Performance Photocatalysis. *Sci. Rep.* **2013**, *3*, 2204.
(34) Hoque, M. A.; Higgins, D. C.; Hassan, F. M.; Chio, J.; Pritzker, M. D.; Chen, Z. Tin Oxide-Mesoporous Carbon Composites as Platinum Catalyst Supports for Ethanol Oxidation and Oxygen Reduction. *Electrochim. Acta* **2014**, *121*, 421−427.

DOI: 10.1021/am5086275
ACS Appl. Mater. Interfaces 2015, 7, 4306−4310